

III-Nitride avalanche photodiodes

Ryan McClintock^a, Jose L. Pau^a, Can Bayram^a, Bruno Fain^a, Paul Giedraitis^a, Manijeh Razeghi^{*a}, and Melville P. Ulmer^b

^aCenter for Quantum Devices, Department of Electrical Engineering and Computer Science, Northwestern University, Evanston, IL USA 60208

^bDepartment of Physics and Astronomy, Northwestern University, Evanston, IL USA 60208

ABSTRACT

Research into avalanche photodiodes (APDs) is motivated by the need for high sensitivity ultraviolet (UV) detectors in numerous civilian and military applications. By designing photodetectors to utilize low-noise impact ionization based gain, GaN APDs operating in Geiger mode can deliver gains exceeding 1×10^7 . Thus with careful design, it becomes possible to count photons at the single photon level. In this paper we review the current state of the art in III-Nitride visible-blind APDs, and present our latest results regarding linear and Geiger mode III-Nitride based APDs. This includes novel device designs such as separate absorption and multiplication APDs (SAM-APDs). We also discuss control of the material quality and the critical issue of *p*-type doping – demonstrating a novel delta-doping technique for improved material quality and enhanced electric field confinement. The spectral response and Geiger-mode photon counting performance of these devices are then analyzed under low photon fluxes, with single photon detection capabilities being demonstrated. Other major technical issues associated with the realization of high-quality visible-blind Geiger mode APDs are also discussed in detail and future prospects for improving upon the performance of these devices are outlined.

Keywords: Avalanche photodiodes, GaN, Photon counting, Photodetector, Ultraviolet

1. INTRODUCTION

Wide bandgap III-nitride semiconductors have been the subject of intense scientific and technological developments since the 1990's, primarily driven by the quest for blue lasers and high brightness visible light emitting diodes.¹ In parallel, III-nitrides have also been studied extensively for use in ultraviolet (UV) photodetectors due to their potential to offer intrinsic visible- or solar-blind detection, which is highly desirable for a number of applications.² Using a visible- or solar-blind detector eliminates the need for expensive and efficiency-limiting optical filters to remove undesired out-of-band visible or solar photons. This makes them well suited for numerous applications in the defense, commercial, and scientific arenas including covert space-to-space communications, early missile threat detection, chemical and biological threat detection and spectroscopy, flame detection and monitoring, UV environmental monitoring, and UV astronomy.^{1,2,3,4}

However, despite the apparent advantages of III-Nitride based photodetectors, many of these applications are still dominated by the use of photomultiplier tubes (PMT). PMTs are capable of obtaining very high sensitivity using internal electron multiplication gain (typically $\sim 10^6$); with proper choice of the photocathode material it is also possible to obtain a degree of visible- or solar-blindness. However these detectors are not without their drawbacks: they are bulky, fragile glass tubes that require large biases (typically 1000 V) to operate effectively.⁵ Therefore, it is highly desirable to develop a compact semiconductor-based photodetector capable of realizing this level of sensitivity.⁶ In principle this can be obtained in III-Nitrides by taking advantage of avalanche multiplication under high electric fields – typically 2.7 MV/cm, which with proper design can correspond to an external reverse bias of less than 100 volts.⁷

Great strides have already been made in the realization of proof-of-concept UV avalanche photodiodes^{8,9,10,11,12} based on III-Nitrides. However, most of the early GaN based APD devices were designed for front-illumination. This configuration makes it possible to use thick GaN templates on sapphire or even silicon. By using thick GaN templates the defect density in the device active region can be reduced. In addition dislocation reduction strategies such as

lateral epitaxial overgrowth (LEO) are possible.¹³ Designing a device for back illumination complicates the design and puts significant limits on the material growth.

Despite the relative ease of growing front-illuminated GaN APDs, the realization of back-illuminated GaN APDs has been demonstrated to be more advantageous.¹⁴ A back-illuminated *p-i-n* GaN structure, in which photons reach the *n*-type layer first, results in primarily the injection of holes into the high-gain multiplication region. This results in higher gain and better overall performance since, near the critical field strength, the hole impact ionization coefficient is higher than the electron impact ionization coefficient in GaN.¹⁵ We have experimentally confirmed this and extracted experimental values for the impact ionization coefficient for holes and electrons in GaN by designing a device that can be operated under either front- or back-illumination, thereby injecting either primarily holes or primarily electrons.¹⁴ In addition, the integration of APD arrays with read-out electronics becomes easier.

In addition to providing higher gain, the design of an APD for back illumination results in an overall lower excess noise factor. This is due to the ionization events being initiated by only holes. This reduces the statistical variation in the avalanche process as it traverses the multiplication region thereby resulting in less observed noise.¹⁴ However, in a normal back illuminated device structure, the absorption of photons does not occur only in the *n*-type layer, and a portion of the photons are absorbed in the multiplication region itself. This means that the gain is not necessarily purely hole-initiated since electrons can be generated by photons absorbed in the multiplication region. This electron contribution to the gain results in lower gain and higher noise than should otherwise be possible. One solution to overcoming this limitation is to modify the design to spatially separate the absorption and multiplication regions by inserting a thin *n*-type separation region. This design is termed a separate absorption and multiplication APD (SAM-APD) structure. The use of separate absorption and multiplication (SAM) regions in avalanche photodiodes is a common approach to reduce multiplication noise and enhance gain through impact-ionization engineering.^{16,17,18} We present the design, fabrication, and characterization of GaN avalanche photodiodes with a separate absorption and multiplication design allowing for nearly pure injection of holes into the multiplication region, offering lower noise performance and higher gain, benefiting from the higher ionization coefficient for holes.

In addition to modifying the device design via impact-ionization engineering for higher performance, it is also crucial to carefully control the material quality and the doping. The breakdown voltage of APDs is largely determined by the electric field build up in the device, and the voltage at which the critical electric field is reached. Because the dark current tends to increase with voltage, reducing the breakdown voltage can be advantageous in achieving higher gains. For a given multiplication width, the primary limitation on the electric field build up is the low carrier concentration of the *p*-GaN layer. The *p*-GaN quality is low due to (1) trade-offs in growth conditions since those at which Mg incorporation is maximized may degrade GaN quality; and (2) the high activation energy of Mg requires that the Mg incorporation in the lattice be almost 100 times higher than the desired carrier concentration leading to a disruption of the GaN lattice.¹⁹ In order to overcome this we have investigated the use of a novel δ -doping technique for the realization of high-quality *p*-GaN.²⁰ Compared to regular bulk *p*-type doping, δ -doped *p*-GaN layers have been shown to have higher structural and electrical quality. By incorporating δ -doped *p*-GaN into a SAM-APD structure we present devices with superior performance.

In addition to realizing high performance linear mode operation, there are many applications that benefit from or even require single-photon detection capabilities from UV detectors. In APDs this can be accomplished through the use of Geiger mode operation. This entails the operation of an avalanche photodiodes well above the breakdown voltage in combination with pulsed quenching circuitry. The electric field chosen to be is sufficiently high that a single charge carrier injected into the multiplication layer triggers a self-sustained avalanche: this current will continue to flow until the avalanche is externally quenched. Geiger-mode operation under gated quenching has been previously demonstrated in front-illuminated GaN APDs with a single photon detection efficiency (SPDE) of 13% at a dark count rate of 400 kHz in devices with an area of 1075 μm^2 .²¹ In contrast, SiC devices have shown a low dark count rate of 28 kHz for much larger 7854 μm^2 devices, but have done this with a lower SPDE of only 3.6%.²² By developing a back-illuminated Geiger mode APD²³, we have realized Geiger mode APDs with a SPDE of 23% and a dark count rate below 10 kHz (our measurement limit).

In this work we review our latest results regarding linear and Geiger mode III-Nitride based APDs. This includes separate absorption and multiplication APDs. We also discuss SAM-APDs that incorporate a δ -doped p -GaN layer for improved performance. The Geiger-mode photon counting performance of our APDs is also discussed.

2. MATERIAL GROWTH AND PROCESSING

2.1. Template Growth

The material was grown in a commercial AIXTRON 200/4-HT horizontal flow low-pressure metalorganic chemical vapor deposition (MOCVD) reactor. In order to allow for back-illumination of the device double-side polished (00.1) sapphire was used as the substrate. Growth on the sapphire substrate was nucleated with a thin 200 Å low-temperature AlN buffer layer. On top of this a 600 nm thick high quality AlN template layer was grown by atomic layer epitaxy^{24,25} at a temperature of $\sim 1300^\circ\text{C}$. This template layer is crucial to realizing high performance back illuminated devices: it allows the active region to be displaced from the highly defected low temperature buffer layer while being completely transparent to wavelengths longer than 210 nm. Atomic force microscopy of the surface of this template shows a well ordered surface with uniform atomic steps clearly visible and a sub-angstrom RMS roughness (Figure 1: left). This layer has an open-detector (00.2) X-ray full-width half-maximum of 41 arc-seconds owing to the excellent crystalline quality of the material.

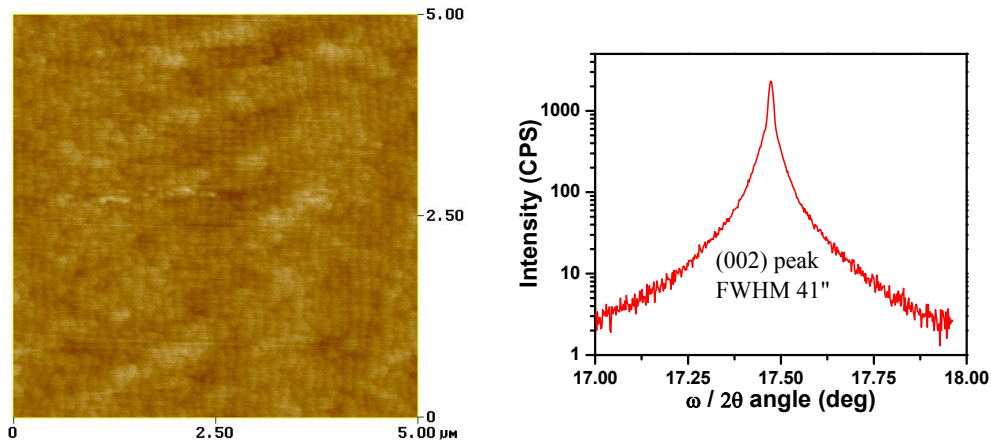


Figure 1. Left) Atomic force micrograph of the surface of a high-quality pulsed atomic layer epitaxially grown AlN template layer (vertical scale = 2.2 nm). Right) Corresponding high-resolution open detector (00.2) $\omega/2\theta$ X-ray diffraction.

2.2. Device Structures

On top of this high quality AlN template layer, the GaN epilayers that make up the device are grown at 100 mBar using hydrogen as the precursor gas. This GaN growth is accomplished without the use of an intermediate buffer layer. The GaN layer surface is very smooth (~ 1.3 Å RMS roughness) with very few observable dislocation termination pits. The active region of the device consists of either a GaN p - i - n or p - i - n - i - n homojunction based structure. The p -type GaN:Mg layer has a hole concentration of $\sim 1 \times 10^{18} \text{ cm}^{-3}$, and it either grown via conventional growth or via δ -doping; the intrinsic GaN multiplication and/or absorption regions have a residual concentration of $\sim 2.5 \times 10^{16} \text{ cm}^{-3}$; and, the intentionally doped n -type GaN:Si layer has a electron concentration of $\sim 2 \times 10^{18} \text{ cm}^{-3}$. A schematic of a conventional APD device structure is shown on the left of Figure 2. The right of Figure 2 shows the SAM-APD structure.

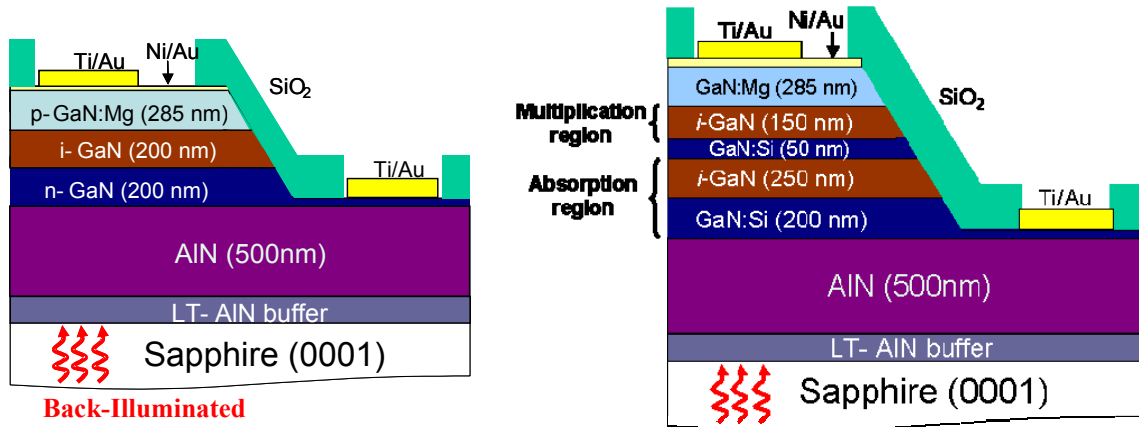


Figure 2. Left) a conventional *p-i-n* APD structure. Right) the separate absorption and multiplication device structure. The GaN:Mg in either structure can be grown either conventionally or via δ -doping.

2.3. Device Processing

All samples are first annealed at 1000 °C for 30 seconds under dry N₂ for magnesium activation of the either conventionally grown or δ -doping grown *p*-type GaN:Mg layer. The material is then patterned into arrays of circular and square detectors with areas ranging from 225 μm^2 up to 14,063 μm^2 using electron cyclotron resonance (ECR-RF) dry etching to reach the bottom *n*-type GaN:Si contact layer. A thin 30 Å Ni / 30 Å Au layer was then deposited on top of the mesas and annealed under ambient air at 500 °C for 10 minutes in order to form ohmic contact to the *p*-type GaN. A 400 Å Ti / 1200 Å Au metal layer was deposited on the GaN:Si layer to form the common *n*-type contact and on top of the thin Ni/Au as a thick metal contact to aid in contacting the device. The devices are finally covered with 300 nm of SiO₂ deposited by plasma enhance chemical vapor deposition to help protect the mesas and prevent premature breakdown of the devices; windows are opened via wet etching.

3. SEPARATE ABSORPTION AND MULTIPLICATION AVALANCE PHOTODIODES

The SAM-APD uses a *p-i-n-i-n* structure as shown on the right of Figure 2. Based upon this structure and the doping described in the growth section, the electric field profile can be calculated from a one-dimensional finite element model. This is shown below on the right of Figure 3 with electric field of a reference structure shown on the left for comparison purposes. At low voltages, the electric field is mainly localized in the topmost *i*-GaN layer (multiplication region). The increase of the reverse bias enhances the electric field in this layer and broadens the depletion region towards the *p*-GaN and across the *n*-GaN layer towards the other *i*-GaN layer. This intrinsic layer becomes fully depleted at the reach-through voltage ($V_{rt} = 40$ V).

3.1. Photon Absorption in SAM-APDs

Absorption measurements performed on reference samples gave a band edge absorption coefficient of $\sim 1 \times 10^5 \text{ cm}^{-1}$. From this value it is possible to calculate the absorption profile of the entire structure when illuminated from the back (assuming no contribution from the sapphire or AlN, or any reflection losses). This is done for both the conventional APD structure and the SAM-APD structure, and plotted below in Figure 3. In the conventional APD structure approximately 75% of the photons are absorbed in the *n*-GaN region, with the remaining 25% being absorbed directly in the intrinsic multiplication region. The exact ratio depends on the electric field, becoming worse at higher electric field strengths. In the SAM-APD structure light absorption in the bottom *n*-GaN and *i*-GaN layers combined account for 99% of the absorption. This results in nearly pure hole-injection into the multiplication region. However, the absorption properties change for photon energies above or below the bandgap²⁶: as the photon energy increases above the bandgap, the light becomes mainly absorbed in the bottom *n*-GaN, closer to the AlN interface; contrarily, as the energy decreases below the bandgap, the light becomes mainly absorbed in the upper layers.²⁷ In particular, the Franz-Keldysh effect may raise the absorption coefficient in the multiplication region at longer wavelengths.²⁸

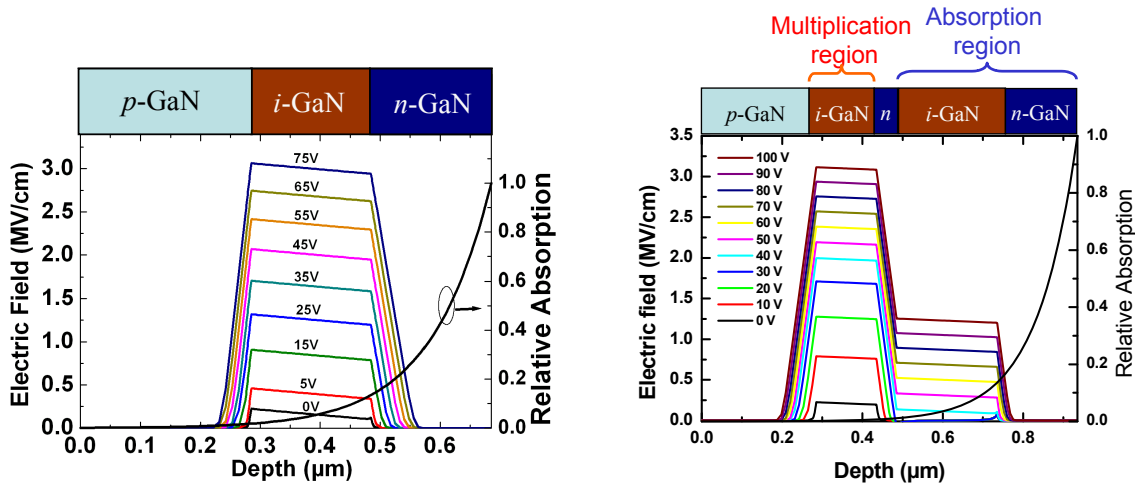


Figure 3. Left) Electric field profile and relative photon absorption profile of a conventional $p-i-n$ APD showing absorption in both the n -GaN and i -GaN layers. Right) Electric field profile and relative photon absorption profile of a SAM-APD showing most of the absorption taking place before photons reach the multiplication region.

3.2. Performance of SAM-APDs

The current-voltage (I - V) characteristics under reverse bias were measured in darkness and under illumination, using the Xe lamp filtered at 360 nm (optical power = 4.1 nW). The light and dark I - V curves were measured alternatively three times in a row to ensure statistically meaningful and consistent device operation. The data is plotted below in Figure 4; the error bars on this figure indicate the standard deviation of the measurements. In darkness, the current remains below the measurement limit up to 30 V. Beyond that voltage, dark current increases monotonously until reaching the breakdown voltage at 95 V, at which point the device exhibits a dark current of 10 nA. At this voltage, the electric field profile predicts an average value of about 3 MV/cm in the multiplication region, in fairly good agreement with the value of the critical electric field in GaN.¹⁴ A sharp increase of the dark current is observed above breakdown reaching 70 μ A at 111 V.

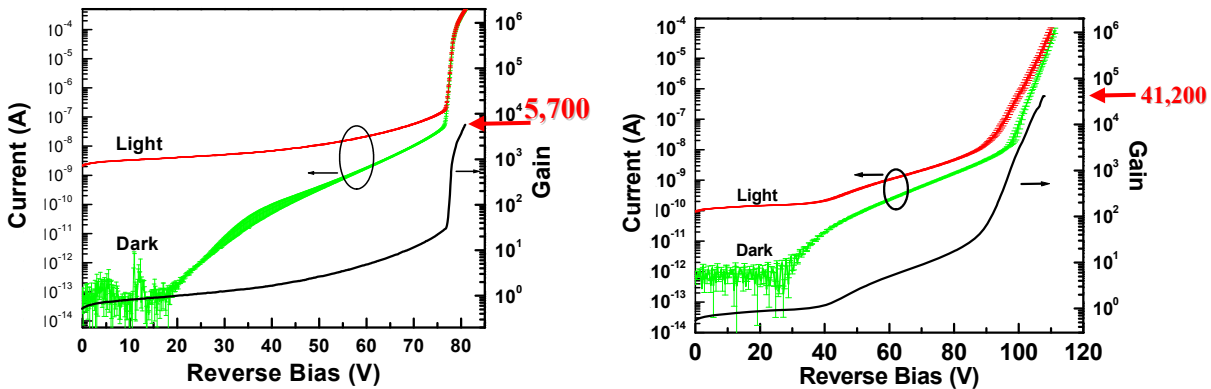


Figure 4. Left) Conventional $p-i-n$ APD I - V curves and gain. Right) SAM-APD I - V curves and gain. In both plots, the left axis shows the measured dark and illuminated currents and the right axis shows the calculated gain.

The current remains fairly flat between zero and the reach-through voltage ($V_{rt} = 40$ V), and then begins to increase with larger reverse bias. To calculate the multiplication gain, we normalized the photocurrent, i.e. difference between light and dark currents, by the difference between the primary un-multiplied current and the un-multiplied dark current. The right axis of Figure 4 shows that the gain increases gradually from V_{rt} . Near the breakdown voltage, the avalanche multiplication gain raises sharply up to a maximum value of 41,200 at 108 V. This represents a significant improvement from our best *p-i-n* APD's maximum gain of 5,700.

The spectral response was measured under back-illumination. At low voltages, the devices present a sharp response at around 364 nm, corresponding to the absorption edge of GaN; the response outside of this peak remains below the background noise of the set-up. This is believed to result from photons are absorbed close to the AlN interface. At the reach-through-voltage of 40 V the depletion region is fully extended, and a peak responsivity of 102.5 mA/W is achieved at 364 nm, corresponding to an external quantum efficiency of greater than 35 %. In addition, the optical response at shorter wavelengths becomes evident in the spectrum.

Noise measurements were performed on these devices in darkness near the breakdown voltage. The signal from the detector was amplified with a low noise trans-impedance amplifier (10^6 - 10^7 V/A), and then analyzed using a fast Fourier transform spectrum analyzer with a 100 kHz bandwidth. The noise characteristic of these devices is dominated by the $1/f$ and multiplication noise contributions at low and medium frequencies, respectively. At low frequencies, the $1/f$ noise increases monotonously as the reverse bias goes over the breakdown voltage (right of Figure 5). At intermediate frequencies, the multiplication noise starts to be evident over the noise floor only above the breakdown voltage. At the same gain level, the contribution of the multiplication noise is considerably lower than the multiplication noise observed in regular back-illuminated *p-i-n* GaN diodes (left of Figure 5).

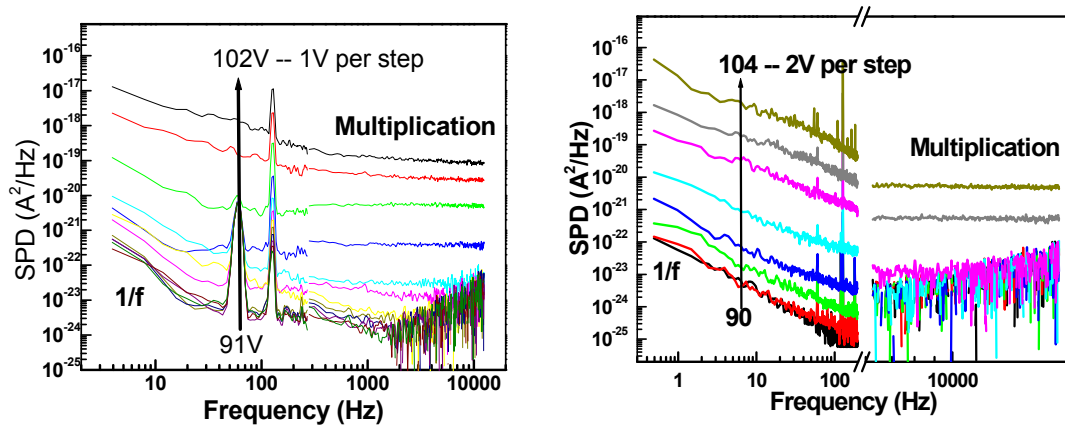


Figure 5. Left) Spectral noise power density (SPD) obtained near breakdown for a standard APD. Right) Spectral noise power density (SPD) obtained near breakdown for a SAM-APD. In both graphs, the broken x-axis separates the low frequency range, in which the $1/f$ contribution dominates, from the mid-frequency range, dominated by the multiplication noise.

In conclusion, the performance of back-illuminated GaN APDs with separate absorption and multiplication regions has been demonstrated and their performance analyzed. In the SAM-APD, higher gain and lower noise than in regular *p-i-n* diodes were achieved through the enhancement of the hole-initiated multiplication.

4. P-TYPE DELTA DOPING FOR IMPROVED APD PERFORMANCE

A number of groups have recently been working to improving *p*-type GaN through the development and optimization of δ -doping.^{29,30,31} In δ -doping the doping profile is implemented as follows: 1) a specific thickness of GaN is deposited normally to grow the GaN period, 2) the TMGa flow is then stopped and the crystal surface is allowed to nitridize, and finally 3) a DCpMg flow is introduced for a specific Mg flow time. The dopant flow is then stopped and TMGa resumed so that the cycle can repeat as the next GaN period is grown.²⁰ This is in contrast to conventional bulk

p-type doping samples, TMGa and DCpMg are supplied together. A schematic diagram of the delta doping scheme is shown below in Figure 6.

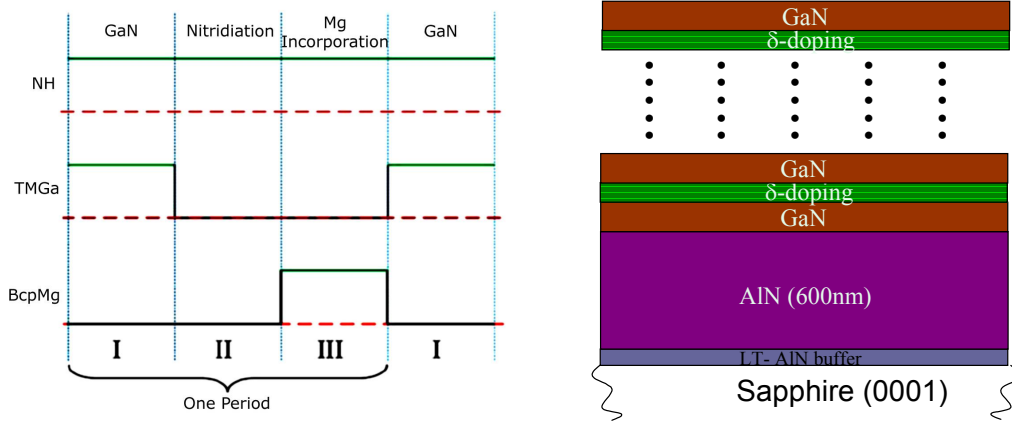


Figure 6. Left) δ -doping precursor profile showing the three step delta doping sequence. Right) Cross-sectional diagram of the δ -doped *p*-GaN test structures used to calibrate the δ -doping.

4.1. Delta doping Optimization

Before growing SAM-APDs with δ -doped *p*-GaN regions, a series of calibration growths were performed to help optimize the δ -doping sequence. A 250 nm layer of *p*-GaN is grown either via conventional bulk growth, or delta-doping on the same 600-nm-thick AlN/LT-AlN buffer/sapphire template used to realize back-illuminated APDs.

The GaN period was initially fixed at 10 nm. The nitridation time was then varied from 15 to 120 seconds; however no significant changes in the hole concentration were observed. Thus, an intermediate nitridation time of 30s was chosen to ensure a stable GaN surface before the Mg flow is introduced. The Mg flow time was then varied from 15 to 60s. With increasing Mg flow time the hole concentration increases and mobility decreases. However for intermediate times the higher hole concentration compensates the mobility decrease leading to a reduction in resistivity with increasing Mg flow time. Comparing the δ -doping with intermediate Mg flow time to the conventional doping, around two orders of magnitude higher doping is achieved by δ -doping under the same growth conditions, with four times lower resistivity. This led us to chose an optimum Mg flow time of 60s. The last experiment was then to vary the GaN period. It was seen that with either larger or smaller periods than the initial 10 nm, the resistivity increases and the hole concentration decreases. For more details on delta doping optimization see ref. 31.

After full optimization, the delta-doping structure is 10 nm of GaN followed by a 30 second nitridation and doped through a 60 s Mg flow time. This results in a *p*-type carrier concentration of $9.4 \times 10^{17} \text{ cm}^{-3}$. A conventionally grown bulk doped structure grown under the same conditions had a significantly lower carrier concentration. However it is possible to obtain carrier concentration in the high 10^{17} or low 10^{18} region by decreasing the growth temperature or increasing the growth pressure.²⁰ However structural characterization of these layers reveals that the quality of the δ -doped *p*-GaN is significantly higher.

4.2. Delta-doped SAM-APDs

The optimized delta doping is then applied to the growth of SAM APDs to investigate the influence of the *p*-GaN quality on the device performance. For comparison a device was also grown using the same growth conditions, but conventionally doping the *p*-GaN layer. The SAM APD structure and processing are the same as discussed in Section 3. After processing, the current-voltage (*I-V*) characteristics under reverse bias were measured in darkness and under illumination, using a Xe lamp filtered at 360 nm using a band-pass filter (optical power = 11 nW). The light and dark

I-V curves are measured alternatively three times in a row to ensure consistent device operation. The resulting measured I-V curves for both devices are shown below in Figure 7 along with the calculated gains. At reach through the δ -doped sample present an average dark current that is a factor of four lower than the dark current obtained in bulk doped sample. This reduction shows the important role the p -GaN layer plays in the origin of the leakage current and confirms the superior quality of the δ -doped samples.

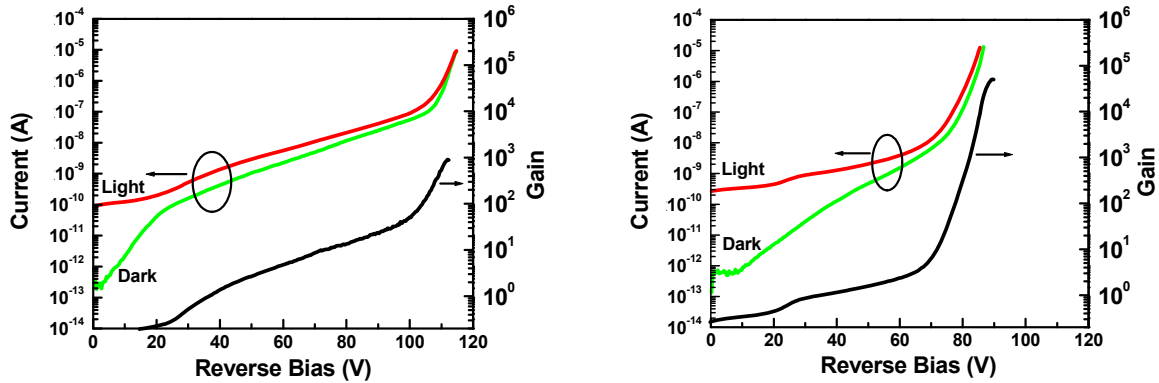


Figure 7. Both devices were grown under identical growth conditions. Left) shows the I-V curves and gain of the conventional bulk p-GaN SAM-APD. Right) Shows the IV curves and gain of the delta-doped SAM-APD. In both plots, the left axis shows the measured dark and illuminated currents and the right axis shows the calculated gain.

The breakdown voltage of the δ -doped SAM-APD is 75 V whereas that of the bulk-doped is 110 V. The difference in breakdown voltage is primarily due to the better confinement of the electric field related to the higher p -doping afforded by the δ -doped p -GaN. A 1-D finite element simulation of the electric field is shown below in Figure 8. Based on this calculation the average electric field in the multiplication region at the onset of breakdown is 2.7 MV/cm in the δ -doped SAM-APD and 2.6 MV/cm in the bulk-doped SAM-APD; both of these are close to their theoretical value.¹⁴ In the delta doped device, after breakdown, the avalanche multiplication reaches a maximum value of 51,000. This is more than 50 times higher than that of the bulk-doped device grown under the same conditions (left of Figure 7). The improvement of the p -GaN quality even enables higher gains than the smaller area SAM APD discussed in Section 3 that was grown with optimized conventional bulk p -GaN doping, thus emphasizing the importance of the high quality δ -doped p -layer.

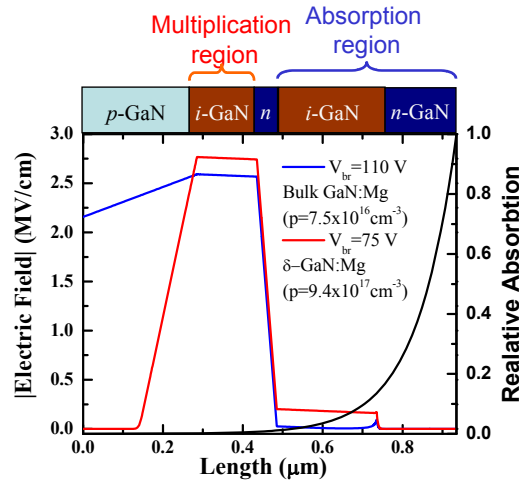


Figure 8. Simulated 1D electric field profiles of the δ -doped (red) and conventional bulk-doped (blue) SAM-APDs devices both biased at their breakdown voltages (V_{BR}).

In conclusion, high quality δ -doped p -GaN has been used to realize ultraviolet back-illuminated SAM-APDs. The higher quality of the δ -doped p -GaN results in lower leakage currents, a lower breakdown voltage, and a higher maximum gain compared to bulk-doped SAM-APD devices.

5. GEIGER MODE AVALANCHE PHOTODIODES

5.1. Experimental setup

The same Xe-lamp and a monochromator setup was used to back-illuminate the devices via a UV fiber-optic cable. The input slit of the monochromator was adjusted to vary the photon flux, which was calibrated using a NIST traceable UV-enhanced Si detector. The APDs were measured in Geiger mode with a gated quenching circuit, as shown in Figure 9. A large reverse DC voltage (V_{DC}) between 74 V and 78 V was applied to the APD through a 47 k Ω current limiting resistor, biasing the device just below breakdown, and a pulsed excess voltage (ΔV_p) between 8.5 V and 10 V was coupled in through a 50 nF capacitor to bias it above breakdown. Pulse repetition rate was 10 kHz with a pulse width of 10 ns and a dead time of 100 μ s.

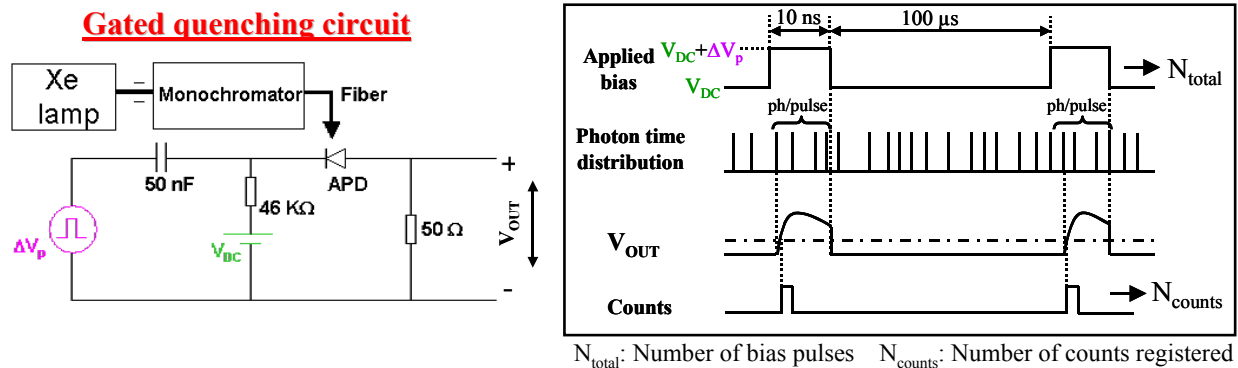


Figure 9. Left) Geiger mode APD testing circuit. Right) diagram of the applied bias, and corresponding output for a given input of photons of approximately 3 photons per pulse.

The device is then illuminated via the fiber optic, and the resulting photocurrent pulses are examined using a Stanford Research model SR400 photon counter for threshold discrimination, and counting of the pulses. The discriminator voltage is chosen to maximize the detection efficiency while minimizing the number of spurious dark counts. The right side of Figure 9 shows a diagram of the various waveforms.

5.2. Photon Counting Operation

The detectors were illuminated with a photon flux of approximately 1 photon per pulse to determine the single photon detection efficiency (SPDE). We also attempted to measure the dark count rate (DCR) by operating the device in the dark, however for the small 225 μm^2 and 625 μm^2 devices, the dark count rate is below the measurement limit of 1 kHz. This low dark count rate suggests that the effect of thermal and tunneling processes on the pulse count is significantly reduced in the small area devices.³² The maximum obtained SPDE was $\sim 23\%$ 625 μm^2 devices. Strangely the smallest 225 μm^2 devices did not perform as well at the larger devices: this may be related to non-linearities as the perimeter to area ratio become sufficiently small.

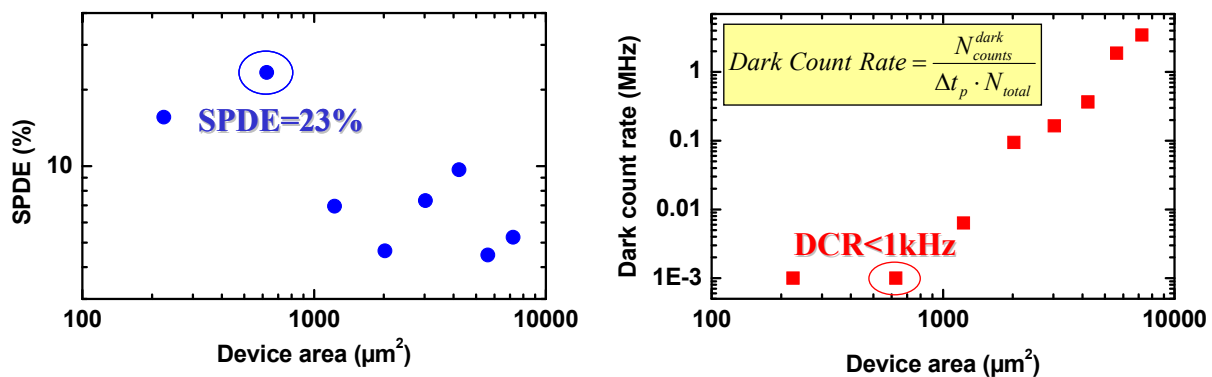


Figure 10. Left) Single photon detection efficiency (SPDE) as a function of diode area showing a maximum SPDE of 23% for 625 μm^2 devices. Right) shows the corresponding dark count rate for these devices. The dark count rate for the smallest two diodes is below the measurement limit.

6. CONCLUSION

In summary, back-illuminated separate absorption and multiplication APDs have been demonstrated. The pure hole injection of a back illuminated SAM-APD resulted in a gain as high as 41,000. By replacing the conventionally doped p -GaN with a novel high-quality δ -doped p -GaN layer the dark current could be reduced and the break down voltage lowered. This resulted in a maximum gain of 51,000. APD devices operating in Geiger-mode capable of single photon counting were also discussed. These devices show a SPDE of 23% and dark count rates $< 1\text{kHz}$.

ACKNOWLEDGEMENTS

J.L. Pau acknowledges the support of the Fulbright Association and the Spanish Ministry of Education and Science. The authors would like to acknowledge Dr. Donald Silversmith (AFOSR), and Dr. Henryk Temkin (DARPA) for their support and encouragement.

REFERENCES

1. M. Razeghi, "Short-wavelength solar-blind detectors- status, prospects, and markets", Proc. IEEE, vol. **90**, pp. 1006-1014, (2002).
2. P. Kung, A. Yasan, R. McClintock, S.R. Darvish, K. Mi, M. Razeghi, "Future of Al_xGa_{1-x}N materials and device technology for ultraviolet photodetectors", Proc. SPIE, vol. **4650**, pp.199-206, (2002).
3. M. Ulmer, M. Razeghi, E. Bigan, "Ultra-Violet Detectors for Astrophysics, Present and Future," Proc. SPIE vol. **2397** pp. 210-216, (1995).

-
4. M. P. Ulmer, R. McClintock, J. L. Pau & M. Razeghi, "A review of UV detectors for astrophysics: past, present, and future," Proc. SPIE Vol. 7222-34 (to be published 2009).
 5. Hamamatsu Photonics, K.K., <http://usa.hamamatsu.com/>, PMTs based upon Cs-Te photocathodes such as R1080.
 6. DARPA BAA06-14, Deep Ultraviolet Avalanche Photodetectors (DUVAP), (2005)
 7. P. Kung, R. McClintock, J. Pau Vizcaino, K. Minder, C. Bayram and M. Razeghi, "III-Nitride Avalanche Photodiodes", Proc. SPIE 6479, 64791J-1-12 (2007)
 8. K. McIntosh, R. Molnar, L. Mahoney, M. Geis, K. Molvar, I. Melngailis, R. Aggarwal, W. Goodhue, S. Choi, and D. Spears, "GaN avalanche photodiodes grown by hydride vapor-phase epitaxy", Appl. Phys. Lett. **75**, 3485 (1999).
 9. J. Carrano, D. Lambert, C. Eiting, C. Collins, T. Li, S. Wang, A. Beck, R. Dupuis, and J. Campbell, "GaN avalanche photodiodes", Appl. Phys. Lett. **76**, 924 (2000).
 10. B. Yang, T. Li, K. Heng, C. Collins, S. Wang, J. Carrano, R. Dupuis, J. Campbell, M. Schurman, and I. Ferguson, "Low dark current GaN avalanche photodiodes", IEEE J. Quantum Electron. **36**, 1389 (2000).
 11. S. Verghese, K. McIntosh, R. Molnar, L. Mahoney, R. Aggarwal, M. Geis, K. Molvar, E. Duerr, and I. Melngailis, "GaN avalanche photodiodes operating in linear-gain mode and Geiger mode", IEEE Trans. Elect. Dev. **48**, 502 (2001).
 12. J.B. Limb, D. Yoo, J.H. Ryou, W. Lee, S.C. Shen, R.D. Dupuis, M.L. Reed, C.J. Collins, M. Wraback, D. Hanser, E. Preble, N.M. Williams, and K. Evans, "GaN ultraviolet avalanche photodiodes with optical gain greater than 1000 grown on GaN substrates by metal-organic chemical vapor deposition", Appl. Phys. Lett. **89**, 11112 (2006).
 13. P. Kung, D. Walker, M. Hamilton, J. Diaz, and M. Razeghi, "Lateral epitaxial overgrowth of GaN films on sapphire and silicon substrates," Applied Physics Letters **74**(4), pp. 570-573 (1999).
 14. R. McClintock, J. L. Pau, K. Minder, C. Bayram, P. Kung, M. Razeghi, "Hole-initiated multiplication in back-illuminated GaN avalanche photodiodes," Applied Physics Letters **90**, 1411121 (2007).
 15. I.J. Oguzman, E. Bellotti, K. Brennan, J. Kolnik, R. Wang, and P. Ruden, "Theory of hole initiated impact ionization in bulk zincblende and wurtzite GaN", J. Appl. Phys. **81**, 7827 (1997).
 16. X. Guo, L. B. Rowland, G. T. Dunne, J. A. Fronheiser, P. M. Sandvik, A. L. Beck, and J. C. Campbell, IEEE Photon Technology Letters, **18**, pp. 136 (2006).
 17. J. C. Campbell, A. G. Dentai, W. S. Holden, and B. L. Kasper, Electronics Letters **19**, pp. 818 (1983).
 18. J. C. Carrano, D. J. H. Lambert, C. J. Eiting, C. J. Collins, T. Li, S. Wang, B. Yang, A. L. Beck, R. D. Dupuis, and J. C. Campbell. Applied Physics Letters **76**, pp. 924 (2000).
 19. P. Kozodoy, S. Keller, S.P. DenBaars, and U. K. Mishra, Journal of Crystal Growth **195**, 265 (1998).
 20. C. Bayram, J. L. Pau, R. McClintock, and M. Razeghi, "Performance enhancement of GaN ultraviolet avalanche photodiodes with p-type delta-doping," Applied Physics Letters **92**(24) pp. 241103-1 (2008).
 21. K. A. McIntosh, R. J. Molnar, L. J. Mahoney, K. M. Molvar, N. Efremow, Jr., S. Verghese, Appl. Phys. Lett. **76**, 3938 (2000).
 22. A. L. Beck, X. Guo, H.-D. Liu, A. Ghatak-roy, J. C. Campbell, Proc. SPIE 6372, 637200-1(2006).
 23. J. L. Pau, R. McClintock, K. Minder, C. Bayram, P. Kung, M. Razeghi, E. Muñoz, and D. Silversmith, "Geiger-mode operation of back-illuminated GaN avalanche photodiodes", Applied Physics Letters **91**(4), 041104 -1 (2007).
 24. R. McClintock, A. Yasan, K. Mayes, D. Shiell, S.R. Darvish, P. Kung, and M. Razeghi, "High Quantum Efficiency Solar-Blind Photodetectors", Proc. SPIE **5359**, 434 (2004).
 25. J. Zhang, H. Wang, W. Sun, V. Adivarahan, S. Wu, A. Chitnis, C. Chen, M. Shatalov, E. Kuokstis, J. Yang, and M. Asif Khan, "High-quality AlGaIn layers over pulsed atomic-layer epitaxially grown AlN templates for deep ultraviolet light-emitting diodes", J. Elect. Mat. **32**, 364 (2003).
 26. J. F. Muth, J. D. Brown, M. A. L. Johnson, Z. Yu, R. M. Kolbas, J. W. Cook, Jr., and J. F. Schetzina, MRS Internet J. of Nitride Semicond. Res., **4S1**, 1 (1999).
 27. E. Monroy, F. Calle, J. L. Pau, F. J. Sanchez, E. Munoz, F. Omnes, B. Beaumont, and P. Gibart, Journal of Applied Physics **88**, 2081 (2000).
 28. K. A. McIntosh, R. J. Molnar, L. J. Mahoney, A. Lightfoot, M. W. Geis, K. M. Molvar, I. Melngailis, R. L. Aggarwal, W. D. Goodhue, S. S. Choi, D. L. Spears, and S. Verghese, Appl. Phys. Lett. **75**, 3485 (1999).
 29. M.L. Nakarmi, K.H. Kim, J. Li, J.Y. Lin, and H.X. Jiang, Applied Physics Letters **82**, 3041 (2003).
 30. C. Simbrunner, M. Wegscheider, M. Quast, Tian Li, A. Navarro-Quezada, H. Sitter, and A. Bonanni, Applied Physics Letters **90**, 142108 (2007).

-
31. C. Bayram, J.L. Pau, R. McClintock and M. Razeghi, "Delta-doping optimization for high quality p-type GaN," *Journal of Applied Physics* **104**(8) pp.083512 (2008).
 32. K. E. Jensen, P. I. Hopman, E. K. Duerr, E. A. Dauler, J. P. Donnelly, S. H. Groves, L. J. Mahoney, K. A. McIntosh, K. M. Molvar, A. Napoleone, D. C. Oakley, S. Verghese, C. J. Vineis, R. D. Younger, *Appl. Phys. Lett.* **88**, 133503 (2006).